Title

Tunable Artificial Relaxor Behavior in [BaTiO3]m/[BaZrO3]n Superlattices

Journal

Physical Review Letters, 130(26)

ISSN

0031-9007

Authors

Tian, Zishen
Xu, Michael
Kim, Jieun
et al.

Publication Date

2023-06-30

DOI

10.1103/physrevlett.130.266801

Tunable Artificial Relaxor Behavior in $[BaTiO_3]_m/[BaZrO_3]_n$ Superlattices

Zishen Tian,[1,2] Michael Xu,[3] Jieun Kim,[1,4] Hao Pan,[1] Djamila Lou,[1] Xiaoxi Huang,[1] James M. LeBeau,[3] and Lane W. Martin[1,2,*]

[1]Department of Materials Science and Engineering, University of California, Berkeley, Berkeley, California 94720, USA
[2]Materials Sciences Division, Lawrence Berkeley National Laboratory, Berkeley, California 94720, USA
[3]Department of Materials Science and Engineering, Massachusetts Institute of Technology, Cambridge, Massachusetts 02139, USA
[4]Department of Materials Science and Engineering, University of Wisconsin, Madison, Madison, Wisconsin 53706, USA

(Received 27 November 2022; accepted 9 May 2023; published 30 June 2023)

$[BaTiO_3]_m/[BaZrO_3]_n$ (m, $n = 4$–12) superlattices are used to demonstrate the fabrication and deterministic control of an artificial relaxor. X-ray diffraction and atomic-resolution imaging studies confirm the production of high-quality heterostructures. With decreasing $BaTiO_3$ layer thickness, dielectric measurements reveal systematically lower dielectric-maximum temperatures, while hysteresis loops and third-harmonic nonlinearity studies suggest a transition from ferroelectriclike to relaxorlike behavior driven by tuning the random-field strength. This system provides a novel platform for studying the size effect and interaction length scale of the nanoscale-polar structures in relaxors.

DOI: 10.1103/PhysRevLett.130.266801

Relaxor ferroelectrics [1] such as $(1-x)PbMg_{1/3}Nb_{2/3}O_3 - (x)PbTiO_3$ and $BaZr_xTi_{1-x}O_3$ draw considerable attention due to their complex physics and use in applications [2,3]. Relaxors are the disordered cousins of long-range-ordered ferroelectrics and possess nanoscale-polar structures instead of ferroelectric domains [4,5]. The existence of chemical disorder in relaxors [6], and hence electric and/or elastic random fields, is understood to be important in producing frustration of long-range polar order and generating their characteristic properties [7,8]. In turn, manipulating chemical order is one of the primary ways to manipulate the polar order of relaxors. For example, it has been demonstrated that annealing $PbSc_{1/2}Ta_{1/2}O_3$ facilitates the growth of chemically ordered regions which leads to a transition from relaxorlike to ferroelectriclike behavior [9], while annealing $PbIn_{1/2}Nb_{1/2}O_3$ leads to a transition to an antiferroelectric phase [10]. Such studies support the connection between chemical order and polar order in relaxors, but several questions remain. Are the nanoscale-polar structures confined in the chemically ordered regions? How does the size of and spacing between the chemically ordered regions affect the collective response of the nanoscale-polar structures? In conventional relaxors, answering these questions is challenging due to the random size and spatial distribution of the chemically ordered regions, which calls for new approaches to exert deterministic control over the chemical order of relaxors.

Approaches to finely control chemical order are now available via modern film-growth techniques that allow for the fabrication of unit-cell precise superlattices [11]. Bearing this in mind, researchers have attempted to produce artificial relaxors such as chemically ordered versions of $PbMg_{1/3}Nb_{2/3}O_3$ (by alternating the growth of $[PbNbO_3]^+$ and $[PbMg_{2/3}Nb_{1/3}O_3]^-$ layers along the [111]) [12] but this proved challenging because of the inherent chemical instability of the $[PbMg_{2/3}Nb_{1/3}O_3]^-$ layers. In this spirit, we consider artificial relaxors based on $BaZr_xTi_{1-x}O_3$ where alternating the growth of the ferroelectric $BaTiO_3$ (with large polarization and long-range order) and dielectric $BaZrO_3$ (with small, unordered polarization and short-range order) [13–15] should enable spatial confinement of the nanoscale-polar structures in the $BaTiO_3$ layers and tuning of the spacing in between by the $BaZrO_3$ layers. Earlier studies of $[BaTiO_3]_m/[BaZrO_3]_n$ superlattices [16,17] revealed the ability to tune the nature of properties and strain and suggest the potential to produce relaxorlike behavior, but details of that potential evolution remain to be fully developed. Ultimately, this system should provide a novel platform for exploring spatial-confinement effects on the nanoscale-polar structures, as well as tuning the coupling between the neighboring layers of nanoscale-polar structures.

Here, we investigate $BaZr_{0.5}Ti_{0.5}O_3$ solid-solution films and $[BaTiO_3]_m/[BaZrO_3]_n$ superlattice heterostructures (including both *symmetric* [$m/n = 4/4, 8/8, 12/12$ unit cells] and *asymmetric* [$m/n = 4/4, 8/4, 12/4$ unit cells] series). Heterostructures with a total thickness of 65 nm were grown via pulsed-laser deposition with *in situ* reflection high-energy electron diffraction (RHEED) (see Supplemental Material for details [18]). All heterostructures were grown either directly on $(LaAlO_3)_{0.3}(Sr_2AlTaO_6)_{0.7}$ (LSAT) (001) substrates (for in-plane studies) or on 35-nm-$La_{0.7}Sr_{0.3}MnO_3$-buffered LSAT (001) substrates

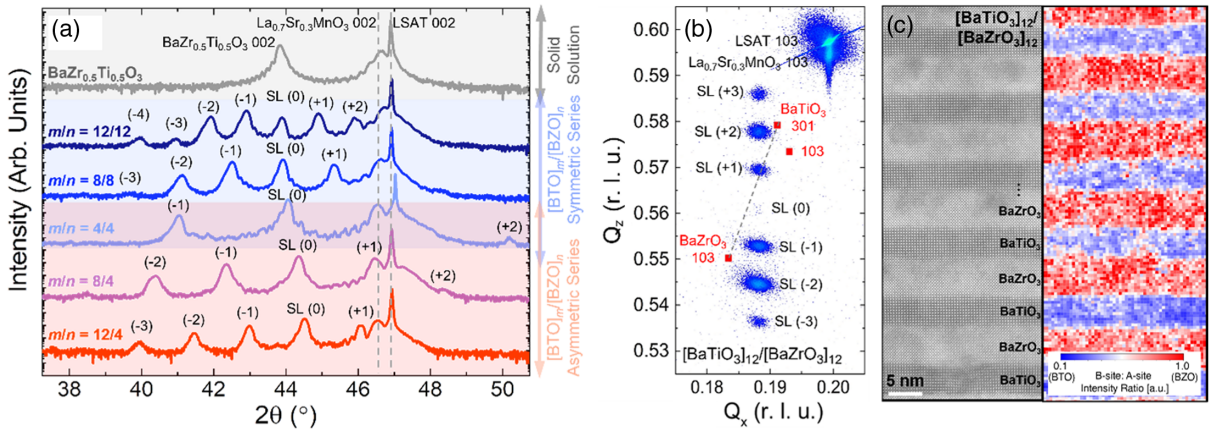

FIG. 1. (a) X-ray θ-2θ scan for the $BaZr_{0.5}Ti_{0.5}O_3$ film and the $[BaTiO_3]_m/[BaZrO_3]_n$ superlattices. (b) X-ray reciprocal space mapping for the $m/n = 12/12$ superlattice near the 103-diffraction condition. The expected position for bulk $BaZrO_3$ and both c and a orientations of bulk $BaTiO_3$ are marked as red squares. (c) Left side: cross-sectional HAADF-STEM images for an $m/n = 12/12$ superlattice. Right side: mapping of the B-to-A-site cation intensity ratio.

(for out-of-plane studies). Given that both $BaTiO_3$ ($a = 3.99$ Å, $c = 4.03$ Å) and $BaZrO_3$ ($a = 4.19$ Å) have considerably larger lattice parameters than LSAT ($a = 3.87$ Å), we anticipated complete strain relaxation. RHEED patterns during growth suggest a layer-by-layer growth mode with the possible existence of two-level or multilevel stepped surfaces [19] (Supplemental Material, Fig. S1 [18]). Following growth, x-ray diffraction θ-2θ line scans [Fig. 1(a)] confirm epitaxial growth and reveal clear superlattice peaks for all heterostructures (see Supplemental Material for details [18]). The solid solution exhibits a single peak close to the expected lattice parameter ($a = 4.10$ Å). For the symmetric superlattice series ($m/n = 4/4, 8/8, 12/12$), the SL(0) peaks vary little in position, suggesting minimal changes in the out-of-plane lattice parameter. For the asymmetric series ($m/n = 4/4, 8/4, 12/4$), however, the SL(0) peak position shifts to higher angles as m increases, which matches the expectation that the average out-of-plane lattice parameter decreases as the fraction of $BaTiO_3$ increases. X-ray reciprocal space mapping studies [Fig. 1(b)] (see also Supplemental Material, Fig. S2 [18]) confirm that the heterostructures are relaxed from the substrate (as expected) and, further, reveal no splitting of the superlattice peaks, indicating that the $BaTiO_3$ and $BaZrO_3$ layers have established an equilibrium strain state with *one another* (but not the substrate) wherein the $BaTiO_3$ is under tensile strain and the $BaZrO_3$ is under compressive strain (+2.2% and −2.1%, respectively, for the symmetric superlattices).

Further structural characterization was performed to reveal the nanoscale chemical order. Cross-sectional scanning transmission electron microscopy images were acquired (see Supplemental Material for details [18]) for the $m/n = 4/4$ and $12/12$ superlattices. Atomic-resolution high-angle annular dark-field (HAADF) images [left, Fig. 1(c)] (see also Supplemental Material, Fig. S3 [18]) reveal alternating brighter ($BaZrO_3$) and darker ($BaTiO_3$) layers; consistent with the expected Z-contrast difference between the zirconium and titanium B-site cations. To extract information about the strain in each layer, in-plane and out-of-plane atomic distances were extracted from the HAADF images (Supplemental Material, Fig. S4 [18]). While the in-plane atomic distance is identical across all the layers (e.g., 4.10 Å for the $m/n = 12/12$ superlattices), the out-of-plane atomic distance oscillates between the $BaTiO_3$ and $BaZrO_3$ layers (4.07 and 4.26 Å, respectively, for the $m/n = 12/12$ superlattices). This confirms that the stacking layers are strained to each other but relaxed from the substrate. In addition, to probe the distribution of Ti^{4+} and Zr^{4+} cations, maps of B-to-A-site intensity ratio [right, Fig. 1(c)] were extracted and reveal well-defined titanium- and zirconium-rich layers with relatively low levels of interdiffusion. This point is confirmed by energy-dispersive x-ray spectroscopy which shows relatively sharp interfaces between layers (Supplemental Material, Fig. S5 [18]). All told, while a small degree of interdiffusion occurs at the interface (as is typical [26]), the superlattices are intact and of good quality. These results demonstrate chemical-order control, and beg the question of how this artificially designed chemical order shapes the collective response of the nanoscale-polar structures?

Aiming to study the macroscopic effects of the microscopic chemical order, dielectric permittivity was measured as a function of frequency and temperature along both the out-of-plane [001] and in-plane [100] [Fig. 2] (see Supplemental Material for details [18]). The out-of-plane dielectric response in the superlattices is strongly suppressed compared to that in the solid solution, which can be (naively) understood based on a capacitors-in-series model. The $BaZrO_3$ layers (which have small dielectric constant $\varepsilon_r \approx 35$ [13]) are in series with the $BaTiO_3$ layers (which have higher values [27]), which limits the overall dielectric

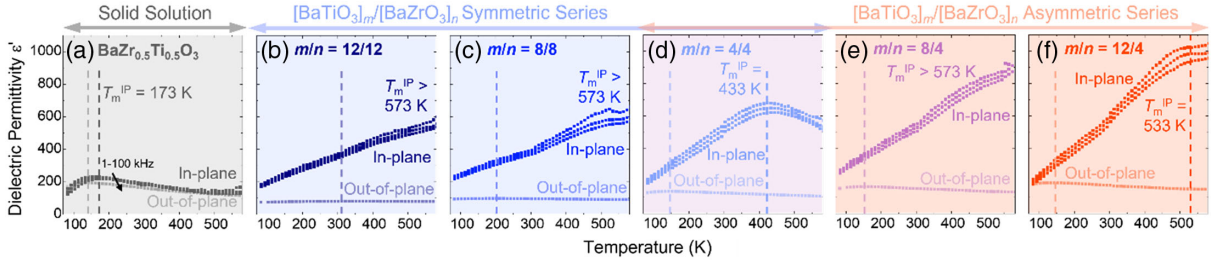

FIG. 2. Dielectric permittivity as a function of temperature for (a) the $BaZr_{0.5}Ti_{0.5}O_3$ film and (b)–(f) the $[BaTiO_3]_m/[BaZrO_3]_n$ superlattices. The measurements were performed along the in-plane [100] and the out-of-plane [001] directions, with field amplitude 0.5 kV cm^{-1} and frequency 1, 10, 100 kHz. Dielectric maximum temperatures extracted from in-plane and out-of-plane measurements ($T_m^{\mathrm{IP}}, T_m^{\mathrm{OOP}}$) are labeled as dashed lines.

response. The opposite is observed for the in-plane dielectric response where the $BaZrO_3$ and $BaTiO_3$ layers are effectively in a parallel configuration and the $BaTiO_3$ layers contribute significantly to the total response. Furthermore, the trend of higher dielectric responses in superlattices with higher $BaTiO_3$ fractions ($m/n = 8/4$ and $12/4$) and similar response in superlattices with identical average composition ($m/n = 4/4, 8/8$, and $12/12$) again confirms that the major contribution comes from the $BaTiO_3$ layers. Another trend is that the superlattices with thinner $BaTiO_3$ layers exhibit lower dielectric-maximum temperature T_m. For example, the $m/n = 8/8$ and $12/12$ superlattices exhibit $T_m(10\ \mathrm{kHz}) > 573$ K which is reduced to 433 K for the $m/n = 4/4$ superlattices. All superlattices, however, have T_m higher than the Curie temperature of $BaTiO_3$ single crystals (393 K [27]). This can be explained by a combination of strain and size effects. The tensile strain in the $BaTiO_3$ layer is expected to enhance the transition temperature (the calculated transition temperature for $BaTiO_3$ with $+2\%$ strain is ~800 K [28,29]), while the finite thickness of the layers (4–12 unit cells) plus the existence of interfaces with nonpolar layers likely act to destabilize the polar phase. Especially, in the superlattice with the smallest periodicity ($m/n = 4/4$), the strong confinement of the polar layers and the high density of interfaces result in the lowest T_m. These observations strongly suggest that the artificially designed chemical order produces significant effects in the dielectric response.

Taking things one step further, to connect the dielectric response to the nanoscale-polar structures, we examined the in-plane temperature-dependent dielectric permittivity of the $m/n = 4/4$ superlattices [Fig. 2(d)] and observed a frequency dependence of T_m. This is a telltale feature of relaxor behavior which is further confirmed by polarization-electric field hysteresis-loop measurements (see Supplemental Material for details [18]). For all superlattices, the hysteresis loops measured along the out-of-plane [001] appear to be nearly linear dielectriclike, while the ones measured along the in-plane [100] show nonlinearity and hysteresis [Figs. 3(a)–3(f)], suggesting the existence of in-plane aligned polar structures and consistent with the tensile strain in the $BaTiO_3$ layers [29,30]. Noticeably, the thicker the $BaTiO_3$ layers, the more ferroelectriclike the hysteresis loops (e.g., $m/n = 12/12$ [Fig. 3(b)] and $12/4$ [Fig. 3(f)]) while those superlattices with thinner $BaTiO_3$ layers exhibit slim, tilted hysteresis loops suggesting relaxorlike behavior (e.g., $m/n = 4/4$ [Fig. 3(d)]). These results hint at a crossover from ferroelectriclike to relaxorlike behavior, but a more sensitive approach is required to determine whether a superlattice is truly ferroelectriclike or relaxorlike.

For this purpose, third-harmonic nonlinearity measurements [20,31] were performed along the in-plane [100] to distinguish between relaxorlike and ferroelectriclike behavior [Figs. 3(g)–3(l)]. Note that, except for the solid solution [Fig. 3(g)], nonlinearity measurements along the out-of-plane [001] are trivial due to the linear-dielectric nature along that direction. When an oscillating electric field $E = E_{\mathrm{ac}}\cos(\omega t)$ is applied to a material, the response has the general form of

$$R = R_0 + R_1\cos(\omega t + \theta_1) + R_2\cos(2\omega t + \theta_2) + R_3\cos(3\omega t + \theta_3) + \cdots$$

with both linear and nonlinear terms [20]. The phase angle in the third-harmonic term (θ_3) is especially important as it carries information about the shape of the hysteresis loops at small fields, from which the mechanism of polarization switching can be inferred. Responses that produce $\theta_3 = -180°$ originate from either reversible domain-wall motion or nanoscale-polar-structure reorientation, while responses that produce $\theta_3 = -90°$ originate from irreversible domain-wall motion. With increasing E_{ac}, θ_3 should shift from $-180°$ to $-90°$ for ferroelectrics (due to the onset of ferroelectric switching) [20,31], and from $-180°$ to $0°$ for relaxors (due to the saturation of nanoscale-polar-structure contributions) [20,31,32]. At small fields, the third-harmonic response from the substrate is non-negligible, which gives $\theta_3 \approx 0°$ (Supplemental Material, Fig. S6(c) [18]). Other than this small-field behavior, the $BaZr_{0.5}Ti_{0.5}O_3$ solid-solution films follow

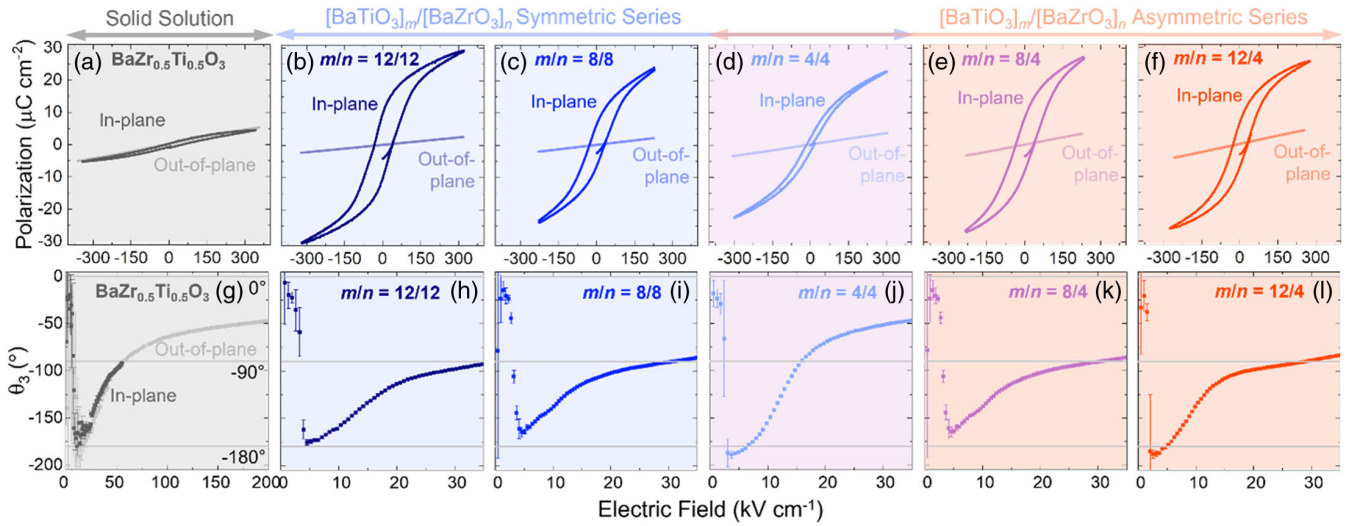

FIG. 3. (a)–(f) Polarization-electric field hysteresis loops for the $BaZr_{0.5}Ti_{0.5}O_3$ film and the $[BaTiO_3]_m/[BaZrO_3]_n$ superlattices. The measurements were performed along the in-plane and the out-of-plane directions, at room temperature and 1 kHz frequency. (g)–(l) Third-harmonic phase angle (θ_3) for the solid-solution film and the superlattices. As the benchmark, both in-plane and out-of-plane studies were conducted at 78 K for the solid solution, while in-plane studies at room temperature were conducted for the superlattices. The measurements were performed at 10 kHz.

the expectation for relaxors, where θ_3 approaches 0° under large electric fields [Fig. 3(g)]. A similar phase-angle shift appears in the $m/n = 4/4$ superlattices, where the in-plane θ_3 exhibits a shift from −180° to −47° over the range of 0–35 kV cm^{-1} [Fig. 3(j)]; supporting evidence that these superlattices have relaxorlike response. In contrast, for all other superlattices, the phase angle saturates near −90°. The in-plane θ_3 for the $m/n = 12/12$ superlattices, for example, exhibits a shift from −180° to −92° over 0–35 kV cm^{-1} [Fig. 3(h)]; consistent with what is expected for a ferroelectric.

In general, both the hysteresis loops and the third-harmonic nonlinearity point at a difference between the $m/n = 4/4$ superlattices and the others. As the $BaTiO_3$-layer thickness is reduced, the in-plane response appears to be more relaxorlike. Two mechanisms may contribute to the frustration of long-range polar order inside the $BaTiO_3$ layers. First, the long-range polar order is broken (or weakened) at the interface layers between $BaTiO_3$ and $BaZrO_3$, and the diminished polarization of these layers couples with the local polarization of the inner $BaTiO_3$ layers. The coupling disrupts the long-range polar order in the inner layers, meaning that each layer experiences a slightly different polar order which, when added together, replicates the physics and phenomena of a relaxor material and the polar nanostructures therein. Second, thermal fluctuations drive the local polarization to deviate from the average polarization, which is greatly exacerbated in ultrathin layers of $BaTiO_3$ [33]. Such fluctuations destabilize the long-range polar order and produce fluctuating nanoscale-polar structures. Both effects are likely to be further enhanced as the thickness of the polar layers is reduced.

In the following, the combined effect of the mechanisms is studied by evaluating the effective random fields in the heterostructure. Conceptually, as the polar-layer thickness is reduced, the random fields are strengthened which eventually destabilizes the long-range order, begging the question of at which point the random fields dominate. Aiming at quantitative understanding of the evolution of random-field strength, the third-harmonic nonlinearity data are fitted to the spherical random-bond-random-field (SRBRF) model, which can explain the nonlinear response of relaxors [21,34]. This model is derived based on an analogy between relaxors and spin glasses, where each nanoscale-polar structure is abstracted as a pseudospin $\vec{S_i}$ subject to random interactions between nearest neighbors and random fields. The Hamiltonian is written as

$$\mathscr{H} = -\frac{1}{2}\sum_{ij} J_{ij}\vec{S_i}\cdot\vec{S_j} - \sum_i \vec{h_i}\cdot\vec{S_i} - g\sum_i \vec{E_i}\cdot\vec{S_i},$$

where J_{ij} denotes the interaction strength between pseudospins $\vec{S_i}$ and $\vec{S_j}$, which follows a normal distribution $N(J_0, J^2)$ with mean J_0 and standard deviation J, h_i denotes the random-field effect on pseudospin $\vec{S_i}$ which follows a normal distribution $N(0, \Delta)$ with zero mean and standard deviation $\sqrt{\Delta}$, and g is a factor proportional to the average dipole moment of each nanoscale-polar structure. The solution to this model [21]

$$P = \beta(1-q)(J_0 P + gE),$$
$$q = \beta^2(1-q)^2(J^2 q + \Delta) + P^2$$

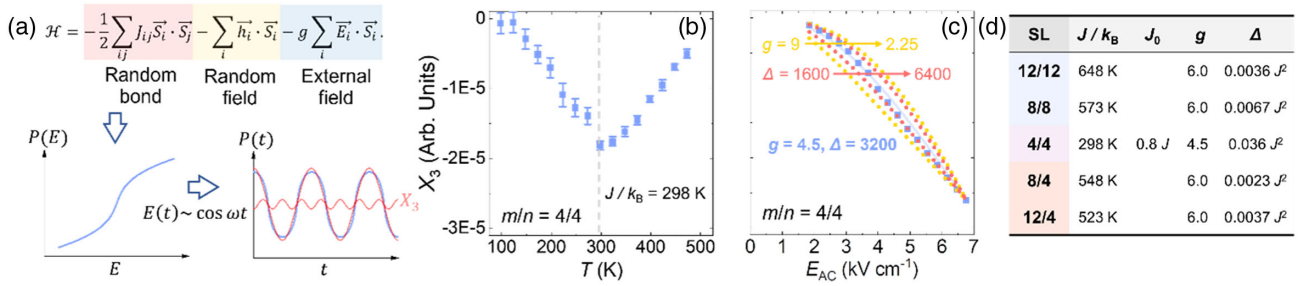

SL	J/k_B	J_0	g	Δ
12/12	648 K		6.0	0.0036 J^2
8/8	573 K		6.0	0.0067 J^2
4/4	298 K	0.8 J	4.5	0.036 J^2
8/4	548 K		6.0	0.0023 J^2
12/4	523 K		6.0	0.0037 J^2

FIG. 4. Quantitative analysis based on the spherical-random-bond-random-field (SRBRF) model. (a) A diagram of calculating the third-harmonic response (X_3) from the model. First the $P(E)$ relation will be solved, then $P(t)$ will be simulated under a cosine-wave electric field $E(t)$, and finally X_3 will be extracted via Fourier transform. (b) X_3 measured as function of temperature, under 5 kV cm^{-1}, 10 kHz oscillating field. The peak position of X_3 is extracted as J. (c) X_3 measured as function of field amplitude, at room temperature and 10 kHz frequency. The best parameters are extracted as g and Δ. (d) Extracted parameters for all the superlattice geometries.

describes the polarization (P) evolution with electric field (E) with four parameters J_0, J, g, and Δ. The third-harmonic response can be predicted as well given the $P(E)$ relationship [Fig. 4(a)].

Here, the in-plane third-harmonic response was measured for all superlattices, at different temperatures T and ac-field amplitudes E_{ac}. Specifically, the in-phase component of the third-harmonic response $X_3 = R_3 \cos\theta_3$ was analyzed, because only this component contributes to the characteristic $-180°$ or $0°$ responses in relaxors. The out-of-phase component $Y_3 = R_3 \sin\theta_3$ was found to be negligible in the range of study (0–7 kV cm^{-1}, see Supplemental Material, Fig. S8 [18]). First, we utilize the knowledge that the third-harmonic response peaks at $T = J/k_B$ [35] and convert the peak position of $X_3(T)$ to the parameter J [Fig. 4(b)] (also see Supplemental Material, Fig. S9 [18]). Next, we assume $J_0 = 0.8J$, and fit the $X_3(E_{ac})$ data to extract the parameters g and Δ [Fig. 4(c)] (also see Supplemental Material, Fig. S10 [18]). It was found that in both the symmetric- and the asymmetric-superlattice series, smaller $BaTiO_3$ layer thickness results in significantly lower J and higher Δ [Fig. 4(d)] which suggests weakened interactions between the nanoscale-polar structures and strengthened random fields. The significant change of random-field strength between the $m = 8$ and the $m = 4$ superlattices coincides with the transition from ferroelectriclike to relaxorlike behavior and suggests that the random-field strength underlies the observed size effect and drives the ferroelectric-to-relaxor transition.

Altogether, artificial relaxors based on $[BaTiO_3]_m/[BaZrO_3]_n$ superlattices allow for the deterministic control of the chemical order via separate tuning of the thickness and spacing of the polar layers. Hysteresis-loop and third-harmonic measurements indicate a transition from ferroelectriclike to relaxorlike behavior between $m = 8$ and $m = 4$. Quantitative analysis of the third-harmonic nonlinearity reveals a significant increase of random-field strength at the crossover, which likely explains the mechanism of the transition. These findings suggest that the nature of polar order can be arbitrarily designed in these artificial relaxors, providing a novel platform for studying the complex physics in relaxors.

Z. T. acknowledges support from the U.S. Department of Energy, Office of Science, Office of Basic Energy Sciences, under Award No. DE-SC-0012375 for the development of superlattice structures with exotic dipolar textures. J. K. acknowledges support from the Army Research Office under the ETHOS MURI via cooperative agreement W911NF-21-2-0162. M. X., H. P., J. M. L., and L. W. M. acknowledge support from the Army/ARL via the Collaborative for Hierarchical Agile and Responsive Materials (CHARM) under cooperative agreement W911NF-19-2-0119. D. L. acknowledges support from the Army Research Office under Grant No. W911NF-21-1-0118. X. H. acknowledges the support from SRC-JUMP ASCENT center. This work made use of the MIT.nano Characterization Facilities.

*lwmartin@berkeley.edu

[1] L. E. Cross, Ferroelectrics **76**, 241 (1987).
[2] A. A. Bokov and Z.-G. Ye, J. Mater. Sci. **41**, 31 (2006).
[3] F. Li, S. Zhang, D. Damjanovic, L. Q. Chen, and T. R. Shrout, Adv. Funct. Mater. **28**, 1801504 (2018).
[4] G. Xu, Z. Zhong, H. Hiraka, and G. Shirane, Phys. Rev. B **70**, 174109 (2004).
[5] A. Kumar, J. N. Baker, P. C. Bowes, M. J. Cabral, S. Zhang, E. C. Dickey, D. L. Irving, and J. M. LeBeau, Nat. Mater. **20**, 62 (2021).
[6] C. A. Randall and A. S. Bhalla, Jpn. J. Appl. Phys. **29**, 327 (1990).
[7] D. Viehland, S. J. Jang, L. E. Cross, and M. Wuttig, J. Appl. Phys. **68**, 2916 (1990).
[8] V. Westphal, W. Kleemann, and M. D. Glinchuk, Phys. Rev. Lett. **68**, 847 (1992).
[9] N. Setter and L. E. Cross, J. Appl. Phys. **51**, 4356 (1980).
[10] A. Kania, K. Roleder, G. E. Kugel, and M. Hafid, Ferroelectrics **135**, 75 (1992).
[11] R. Ramesh and D. G. Schlom, Nat. Rev. Mater. **4**, 257 (2019).

[12] S. Shetty, A. Damodaran, K. Wang, Y. Yuan, V. Gopalan, L. W. Martin, and S. Trolier-McKinstry, Adv. Funct. Mater. **29**, 1804258 (2019).
[13] T. Maiti, R. Guo, and A. S. Bhalla, J. Am. Ceram. Soc. **91**, 1769 (2008).
[14] C. Laulhé, F. Hippert, R. Bellissent, A. Simon, and G. J. Cuello, Phys. Rev. B **79**, 064104 (2009).
[15] A. R. Akbarzadeh, S. Prosandeev, E. J. Walter, A. Al-Barakaty, and L. Bellaiche, Phys. Rev. Lett. **108**, 257601 (2012).
[16] M. Benyoussef, J. Belhadi, A. Lahmar, and M. El Marssi, Mater. Lett. **234**, 279 (2019).
[17] J. Belhadi, F. Ravaux, H. Bouyanfif, M. Jouiad, and M. El Marssi, Appl. Surf. Sci. **512**, 145761 (2020).
[18] See Supplemental Material at http://link.aps.org/supplemental/10.1103/PhysRevLett.130.266801 for additional experimental details and analysis, which includes Refs. [19–25].
[19] S. Hasegawa, *Characterization of Materials*, 2nd ed. (John Wiley and Sons, New York, 2012), pp. 1925–1938.
[20] L. M. Riemer, L. Jin, H. Uršič, M. Otonicar, T. Rojac, and D. Damjanovic, J. Appl. Phys. **129**, 054101 (2021).
[21] R. Pirc and R. Blinc, Phys. Rev. B **60**, 13470 (1999).
[22] G. W. Farnell, I. A. Cermak, P. Silvester, and S. Wong, IEEE Trans. Sonics Ultrason. **17**, 188 (1970).
[23] D. Dimos, M. Raymond, R. Schwartz, H. Al-Shareef, and C. Mueller, J. Electroceram. **1**, 145 (1997).
[24] G. H. Gilmer and M. H. Grabow, JOM **39**, 19 (1987).
[25] S. Tsunekawa, K. Ishikawa, Z. Q. Li, Y. Kawazoe, and A. Kasuya, Phys. Rev. Lett. **85**, 3440 (2000).
[26] N. Nakagawa, H. Y. Hwang, and D. A. Muller, Nat. Mater. **5**, 204 (2006).
[27] A. Von Hippel, Rev. Mod. Phys. **22**, 221 (1950).
[28] K. J. Choi, M. Biegalski, Y. L. Li, A. Sharan, J. Schubert, R. Uecker, P. Reiche, Y. B. Chen, X. Q. Pan, V. Gopalan *et al.*, Science **306**, 1005 (2004).
[29] Y. L. Li and L. Q. Chen, Appl. Phys. Lett. **88**, 072905 (2006).
[30] O. Diéguez, S. Tinte, A. Antons, C. Bungaro, J. B. Neaton, K. M. Rabe, and D. Vanderbilt, Phys. Rev. B **69**, 212101 (2004).
[31] S. Hashemizadeh and D. Damjanovic, Appl. Phys. Lett. **110**, 192905 (2017).
[32] S. Shetty, J. Kim, L. W. Martin, and S. Trolier-McKinstry, J. Appl. Phys. **128**, 194102 (2020).
[33] Y. Nahas, S. Prokhorenko, I. Kornev, and L. Bellaiche, Phys. Rev. Lett. **119**, 117601 (2017).
[34] R. Blinc, J. Dolinšek, A. Gregorovič, B. Zalar, C. Filipič, Z. Kutnjak, A. Levstik, and R. Pirc, Phys. Rev. Lett. **83**, 424 (1999).
[35] V. Bobnar, Z. Kutnjak, R. Pirc, R. Blinc, and A. Levstik, Phys. Rev. Lett. **84**, 5892 (2000).